Communications in Physics, Vol. 22, No. 4 (2012), pp. 317-326

DENSITY FUNCTIONAL BASED TIGHT BINDING STUDY ON WURZITE ZnS NANOWIRES

LE THI HONG LIEN, VU NGOC TUOC, NGUYEN THI THUONG
Institute of Engineering Physics, Hanoi University of Technology

Abstract. *We present a semi-abinitio - Density Functional Based Tight Binding (DFTB) study on the atomic and electronic structure of ZnS Nanowire (NW) and examine the dependence of surface stress on nanowire lateral size and shape. The ZnS wurtzite wire size ranges from 10 to 45Å and of various possible shapes - triangular, hexagonal and circular-like. We investigate the role of unsaturated dangling bond state in the region of band gap varying the wire's diameter. We have calculated the surface formation energy and find that it decreases with increasing the wire diameter and a greater stability (lower surface formation energy) comes with hexagonal and circular-like depending on wire's diameter. Other electronics and mechanical properties e.g. density of states (DOS), Young modulus... also are found to depend on the wire's size and shape. Futher the wire passivation by hydrogen has also investigated.*

I. INTRODUCTION

Nanostructured Zinc sulfide (ZnS) materials - one of the richest among all inorganic semiconductors for its nanoscale morphologies, have been the subject of intensive study owing to their distinguished performance in optoelectronics, sensors, transducers, and biomedical sciences [1]. Its atomic structure and chemical properties are comparable to more popular and widely known ZnO. However, certain properties pertaining to ZnS are unique and advantageous over the ZnO, e.g. the band gap of ∼3.72 eV and ∼3.77 eV (for cubic zinc blende (ZB) and hexagonal wurtzite (WZ) ZnS, respectively) that is larger than ZnO (∼3.4 eV) and therefore it is more suitable for visible-blind ultraviolet (UV)-light based devices e.g. sensors/photodetectors. Further, the lack of a centre of symmetry in wurtzite, combined with its large electromechanical coupling, results in strong piezoelectric and pyroelectric properties and the consequent use of ZnS in surface acoustic wave device for communication and sensing applications. Moreover, its bio-safe and biocompatibility may result in many biomedical applications without any coating.

Nanostructured materials are a new class of materials, having dimensions in the 1-100 nm range, providing one of the greatest potentials for improving performance and extended capabilities. Nanostructures can be divided into zero-dimensional (0D), one-dimensional (1D), and two-dimensional (2D) based on their quantum confinement shapes. This work emphasis in 1D nanostructures - an elongated nanowire due to the intriguing possibility of using them in a majority of short-term future applications. In addition, ZnS nanowire can be synthesized using diverse techniques and its ability to manipulate and align these individual nanostructures is necessary for wafer-based large scale integration. ZnS nanowire usually grow along the [0001] direction and have the same structure as

their bulk wurtzite phase [1, 2]. For sufficiently thin ZnS nanowire, quantum size effects are expected to have a dominant influence, e.g. significant enhancement of the exciton binding energy in the colloidal-synthesized ZnS nanowire with average diameter of 2.2 nm and average length of 43 nm was observed, which implies a promising candidate for ultraviolet laser devices operating at room temperature. Since ultra thin ZnS nanowires are single crystalline and nearly defect-free, their high surface-to-volume ratios enhance atomic mobility and promote structural reconstruction. Different from the nanotubes, whose electronic properties are largely determined by the chirality of the nanotube, nanowires have the advantage that many of their properties, particularly electronic structure, can be controlled during growth by varying the size, composition, and growth direction [1, 2].

Zinc-containing systems have been widely investigated by DFT based first-principles methods [3–6], however it become difficult to treat a large number of atoms because of their high computational demands. Therefore, self-consistent charge density-functional tight-binding (SCC-DFTB) method [7–10], which has been successfully applied to large-scale quantum-mechanical simulations, is suitable candidate for the task. The method is an approximation to the Kohn-Sham density-functional theory (DFT), which combines reasonable accuracy and computational efficiency. The present work represents an extensive study of ZnS wurtzite nanowire systems, which we perform using first-principles Density Functional Tight-Binding calculations.

II. MATERIAL

Density Functional Tight-Binding calculations are performed using DFTB+ codes [10], where we employ the periodic boundary condition (PBC) within the slab approach. The [0001] ZnS nanostructures had their growth direction oriented along the z-axis in the supercell for circualr-like cross sections, with vacuum regions was chosen sufficiently large so that the dimension of wire from surface to surface (larger than 10Åin lateral plan) to avoid interaction between the nanowire and its periodic image. Large number of k-points sampling (∼20 points, see Fig. 4) has been used for band structure. It is noted that, the shapes of nanowires are chosen in such a way as to minimize the number of dangling bonds on outer edge-layer atoms, that have a minimum coordination of 3, leaving at most one dangling bond on the edge atoms. The "effective" diameter for circular-like while preserving the hexagonal symmetry shapes is considered as diameter of the circumsribed circle, which in our cases is varying from approximately 30 to 40 Å. From our previous studies [11] we learn that while wire's the outer surface dangling bonds are not saturated then the surface relaxation in a nanowire occurs inevitably compare to that is taken from its stress-free bulk counterpart.

This relaxation may initially deform the nanowire without any applied loads. Therefore, relaxation must be conducted in atomic simulations of nanowires to let them reach thermodynamics equilibrium state in both wire's growth direction [0001] (wire axial) and its perpendicular surface. At a result the bond length at the outermost surface layer along and perpendicular to the wire direction, have been contracted during relaxation (see Fig. 1) causing some shrinkage on the outer wire's surface. This behavior is found across the entire range of diameters and the shapes of nanowires. In this work, we simulate nanostructures of all possible configuration of single crystal wurtzite ZnS NW with

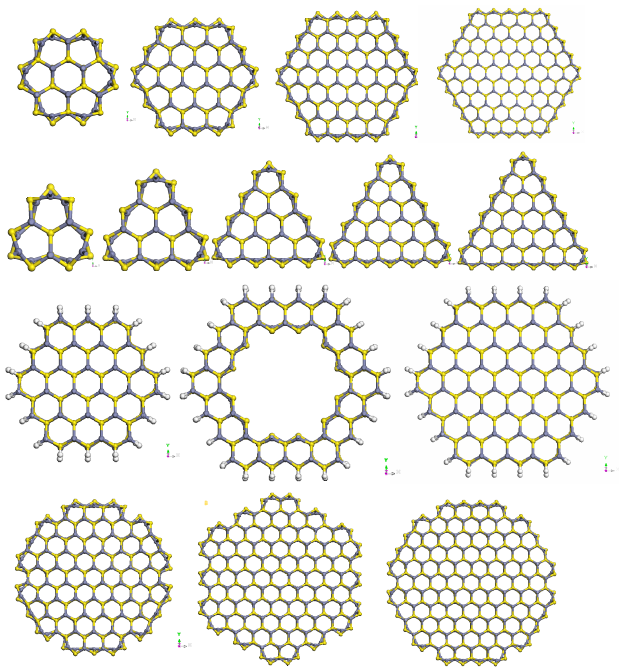

Fig. 1. Relaxed structures of the prismatic NP hexagonal faces ZnS nanowires in [0001] direction.

various size and shape as synthesized experimentally. The wire axis is choosen as (001) wurzite direction. Fig. 1 shows the cross section of relaxed NWs consist of wire wrapped with a vacuum region which was chosen sufficiently large so that the dimension of wire from surface to surface is larger than 10Å(in lateral plan) to avoid interaction between the nanowire and its periodic image. The "effective" diameter is calculater from equi-area of bulk value. Their relaxations show the ourter surface atoms, i.e. facets, are deformed (shrinkage) under larger strain with anion site (Zn) go more inside than cation (S) due to the dangling bonds resulting in a larger charge transfer between Zn and O at the facets (see Fig. 1).

III. DENSITY-FUNCTIONAL-BASED TIGHT-BINDING PLUS (DFTB+) METHOD

The spin-polarized, charge self-consistent, DFTB approach is based on a second-order expansion of the spin-dependent Kohn-Sham total energy functional with respect to a given reference charge and magnetization density. The method has been extensively discussed elsewhere [7–9] and briefly outlined here as:
1/ Expand the orbitals as a linear combination of Slater type orbitals (LCSTO):

$$\psi_n(r) = \sum_{\text{atomicsite}\, i} \sum_{\text{orbital}\, \nu} C_{i\nu}\phi_{i\nu}(\mathbf{r} - \mathbf{R}_i) \tag{1}$$

The basis functions $\phi_{i\alpha}(\mathbf{r}-\mathbf{R}_i)$ centered on the atomic nucleus i, with position $\mathbf{R}_i$, are themselves a linear combination of single Slater orbitals

$$\phi_\nu(\mathbf{r}) = (\sum_{j=1}(\sum_{n=0} a_{jn}\mathbf{r}^{l_\nu+n})e^{-\alpha_j r})Y_{l_\nu m_\nu}.$$

The angular and magnetic quantum number are indicated with l_ν and m_ν. $Y_{l_\nu m_\nu}$ is the corresponding real spherical harmonic.

2/ Tight-binding expansion of the wave functions (calculation of the matrix elements in the two-centers approximation).

$$\sum_{\text{atomic site } i}\sum_{\text{orbital }\nu} |H_{i\nu,j\mu} - ES_{i\nu,j\mu}|\, C_{i\nu,j\mu} = 0 \tag{2}$$

with

$$H_{i\nu,j\mu} = \left\langle \phi_{i\,\nu}|\hat{H}|\phi_{j\,\mu}\right\rangle \tag{3}$$

and

$$S_{i\nu,j\mu} = \langle\phi_{i\,\nu}|\phi_{j\,\mu}\rangle \tag{4}$$

3/ Second order-expansion of Kohn-Sham energy functional (self-consistency in the charge density - SCC-DFTB):

$$E_{tot} = \sum_i^{occ.} n_i \langle\psi_i|\, H_0\, |\psi_i\rangle + \frac{1}{2}\sum_{\mu,\nu}\gamma_{\mu\nu}\Delta q_\mu \Delta q_\nu + E^{rep} \tag{5}$$

where Δq_μ - charge fluctuation decomposed into atomic contribution (Mulliken charge), $\gamma_{\mu\nu}$ - some integral coefficient, E^{rep} - repulsive term (see [6–8]).

With all matrix elements and orbitals are derived from Density Functional calculation, the advantage of DFTB method relies on the use of small basic set of atomic orbitals (in order to reduce the matrix dimension for diagonalization speed-up) and the restriction to two center non-orthogonal Hamiltonian (allowing extensive use of look-up table). What it distinguishes from semi-empirical method is the explicite calculation of the basic wave function which allow deeper physics insight and better control of the approximation used. The method solved Kohn-Sham equation self-consistently using Mulliken charge projection. This approach have proved to give transferable and accurate interaction potential as well as numerical efficiency allowing Molecular Dynamic (MD) simulation of supercell containing several hundreds to a thousand atoms. Thus this is particularly suitable to study the electronics properties and dynamics of large mesoscopic system and organic molecule such as Nano-wire, CNT's, DNA stands or absorbate on surface, semiconductor hetero-structure etc. see review in [7–9, 12] and references there in. The advantage of DFTB parameterization is that only few, possibly well chosen systems are needed to create the parameters, i.e. in DFTB fit systems can also be purely ideal systems, if they are chemically acceptable and can be described carefully with an ab-initio approach. Next this well tested parameter, e.g. in an attention for solid state systems and for defect physics as in current case, can be used for much larger system due to its transferability. In our calculation the parameter and its transferability have been successfully applied in several DFTB works [7–9].

The electronic DFTB parameters (i.e., Hubbard parameters, ν and $S_{\mu\nu}$ matrix elements)

were derived directly from DFT calculations, performed within the generalized gradient approximation (GGA) and using the Perdew, Burke, and Ernzerhof (PBE) exchange-correlation functional.

IV. RESULTS AND DISCUSSION

IV.1. Atomic structure

Examining the nanowires with different diameter and comparing to the bulk value show a contraction of 5.4%-7.2% Zn-S bond along wire's direction. Further at the 1st inner layer from the surface of the nanowires, the contraction is less than 0.6% then within the second layer beneath the surface, similarly less than 0.2%. The other Zn-S bond which forms a zigzag chain from the outermost surface, running perpendicular to the wire direction, also be contracted during relaxation but in less extend which ranging from 2.5% to 5.% and its beneath layer is less than 1.1%. These lengths stabilized and approaching the free surface value with increasing the wire's diameter. These similar behavior also reported for ZnO by us [11] and other, e.g. T. Frauenheim group [12] and D.J. Carter [13].

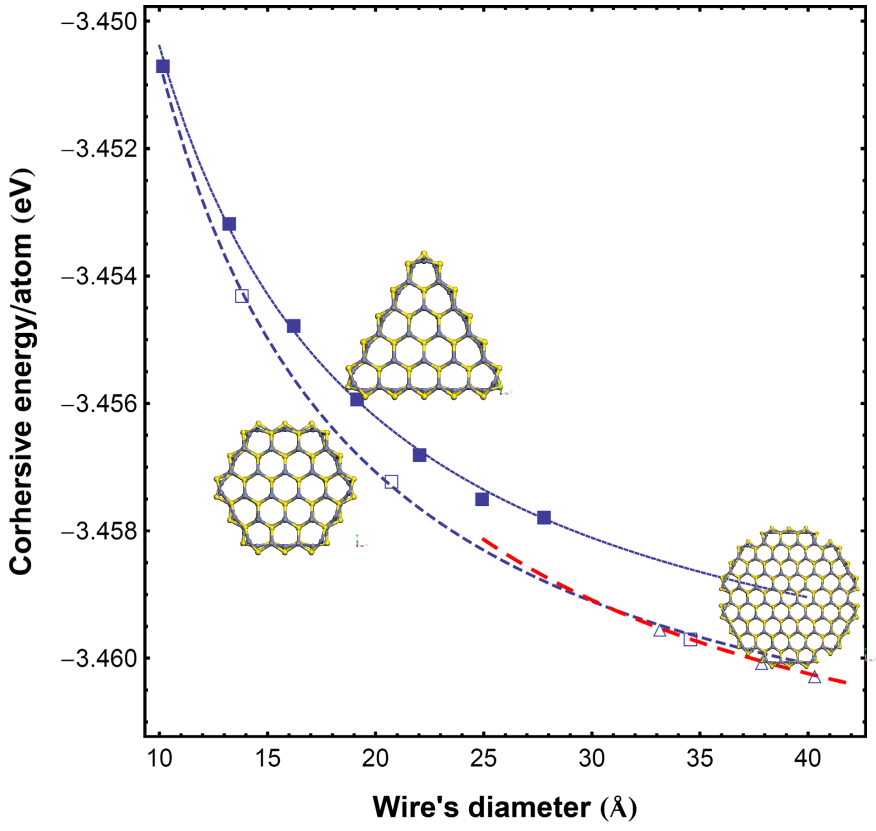

Fig. 2. Diameter dependence of the cohersive energy for the various type ZnS nanowire.

The contraction in Zn-S bond length at the edge of the nanowire derive a corresponding change in bond angles, with the Zn-S-Zn and S-Zn-S of hexagonal nanowires from being 109.2° before relaxation, change to 118°-123° and 105°-108.5°, respectively, after relaxation approaching the free surface value with increasing diameter.

We next calculated the cohersive energy with relative to bulk wurtzite value per atom as a function of diameter. As it can be seen in the Fig. 2 with increasing wire's diameter together with the decreasing of the surface-to-volume ratio the cohersive energy approaches to the bulk optimized value (not shown). Further, it is clear that the most stable wire (energetically) is the hexagonal wire with up to diameter of 35Å however the circular is one for larger (Fig. 2).

IV.2. Uniaxial tensile test on Nanowire

We simulate the tensile-compressive test on wire along their axes as follows: for the purpose of testing the dependence of supercell size we vary the supercell, i.e. as single, double or triple of relaxed lattice constant along the wire axial and choose the double size as more relevant supercell size for taking long range effect (see the inset of Fig. 3). Each nanowire then is carefully elongated or contracted by steps of 0.05 Åfrom its equilibrium state, respectively, followed by fully structural optimization and total energy calculation for each supercell length. In Fig. 3 the inset shows the dependence of strain energy per atom ut versus the applied strain along wire direction and u0 is equilibrium minima. It reveals that the optimized lattice parameter along wire direction has shifted left toward the bulk value while increasing the wire. This is also evident that the wire longitudal size is prolonged compare to the bulk value, which is expected to go along with the contraction in transversal size.

Due to the large surface-to-volume ratio of nanowires, surface effects, e.g surface stress and surface elastic stiffness, are naturally used to explain the size-dependent Young's modulus. To characterize the stiffness under external tension we calculated the Young's modulus of different ZnS nanowires, which is defined by the second derivative of the total energy with respect to the tensile strain at the equilibrium i.e.

$$Y = \frac{1}{V_0}\left(\frac{\partial_2 E}{\partial \varepsilon^2}\right)\Big|_{\varepsilon=0} \tag{6}$$

where E is the total energy, ε is the axial strain, and V_0 is the equilibrium volume obtained from the product of axial equilibrium length (in our slab $l = 2 * c_{relaxed}$) and the cross sectional area S_0 of a nanowire (hexagonal and triangular area shapes). Young's modulus of each nanowires were then determined via parabolic fitting the computed energy-strain curve near the zero strain, which mean $\varepsilon \leq 2.5\%$. Our results are in good accordance with the atomic force microscopy measurements of Young's modulus for ZnS nanowires [14], where the increase in the elastic modulus for the thinner wires is attributed to the surface effect. Various uniaxial tensile test (see inset) have been applied to estimate the Young modulus parameter of wire range from 45-60 GPa (exp. 74.5GPa). Also band gap of uniaxial strained wire allow to estimate piezoelectrical properties of such wurzite NW (results to be published).

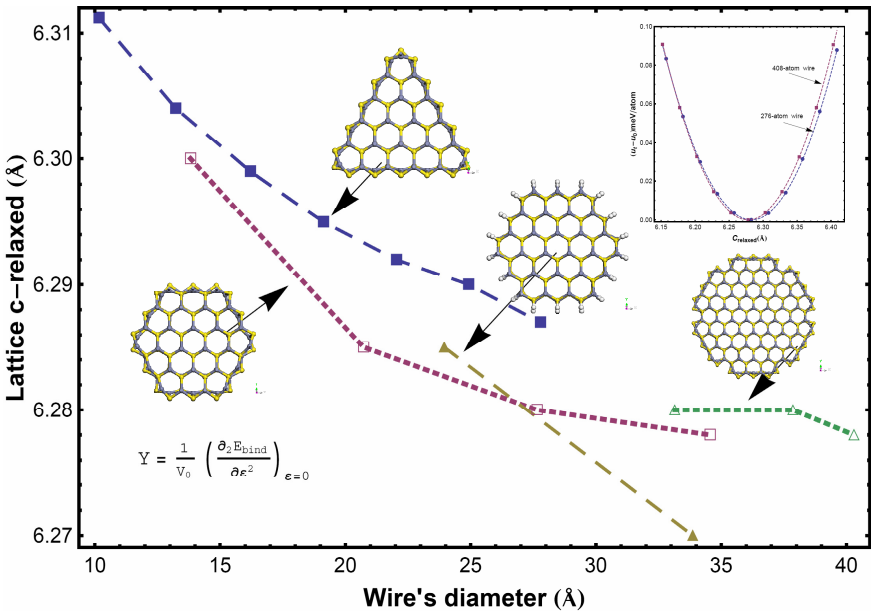

Fig. 3. Relaxed c-lattice prameter of wire's (along wire's direction). The inset show strain energy per atom versus the strained wire lattice parameter. The dashing line is quadratic fitting curve for loading tensile test, from which Young modulus is defined.

IV.3. Bandstructure analysis

Band structures for relaxed nanowires are shown along the Z direction (parallel to wire direction) are shown in Fig. 4. Here, the 1D band structures were computed using $1\times1\times20$ K-points. Similar result is obtained for all sized nanowires, so we have selected two representatives for nanowire. The band gap decreases with increasing nanowire diameter approaching bulk parameter.

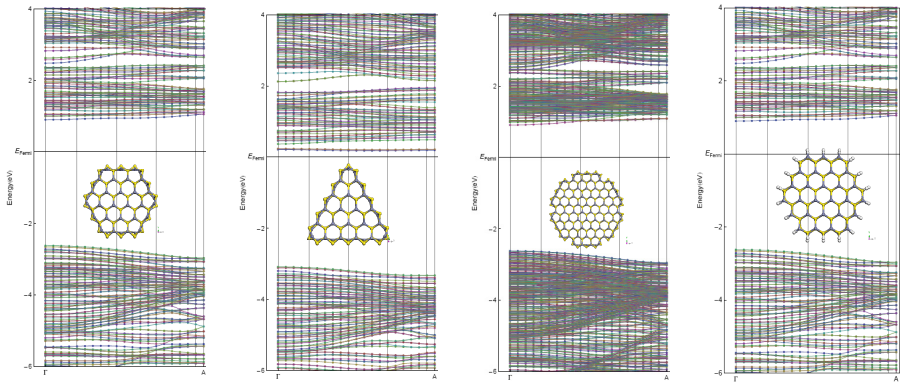

Fig. 4. Relaxed lattice parameters of HS NW along [001] vs wire's diameter.

The band analysis show that the top of valence band does not change much for all the wires, but the bottom of the conduction band moves up as the diameter decreases, which results in the band gap becoming wider. It can be seen that, the bottom of conduction band and the top of valence band were both located in point of the Brillouin zone, indicating a direct band gap semiconductor. This imply the clear dependence between the nanowire diameter and its resulting band gap, which is given as gap's value at the Gamma point (see Fig.5) for direct semiconductor as in the case, so that wire's diameter can be used as one parameter to tailor the band gap for a particular device application.

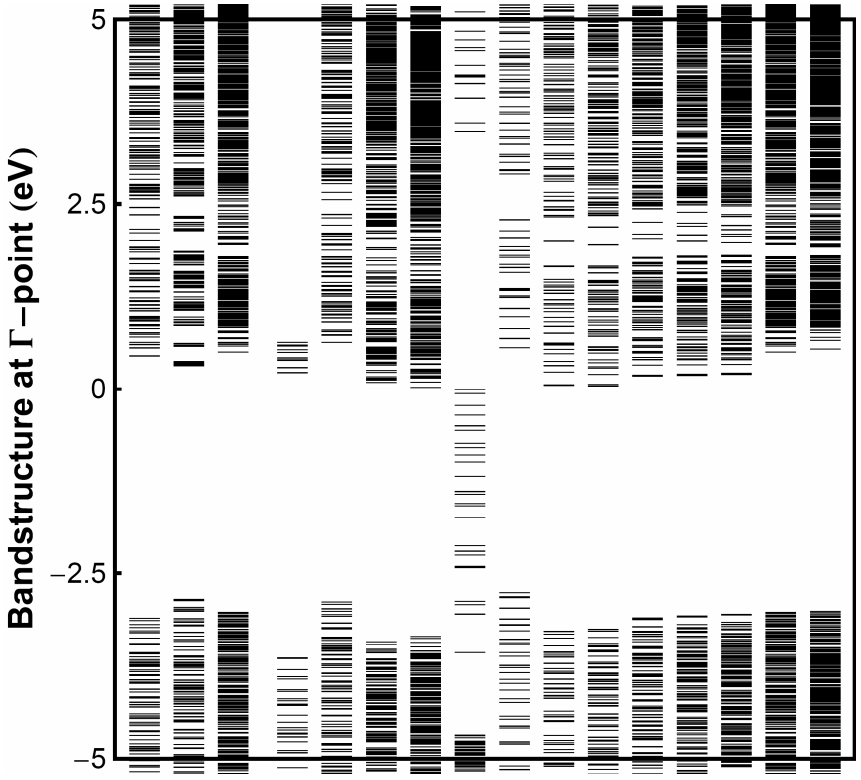

Fig. 5. The band structures for some representative relaxed HS nanowire.

Although it should of course be taken into consideration that band gaps calculated using DFT are systematically underestimated but the trend is reserved. By comparing this picture with unpassivated and hydrogen-passivated wire it can be seen the existence of several in-gap surface states. Further from the k-dependence one can calculate the effective mass of electron and hole along wire direction, with respect to the free electron mass m_0, around the Conduction Band Minimum (CBM) and Valence Band Maximum (VBM) using the expression

$$\Delta E_{c/\nu}(k) = \pm \frac{\hbar^2 k^2}{2m^*_{e/\hbar}} \tag{7}$$

by fitting a quadratic form near the band edges. We examine the dependence of the effective mass on nanowire diameter which increasing as the diameter increases approaching to bulk value of $0.21m_0$. Thus we may expect on some improvement of the mobility for ultrathin wire due to its smaller effective mass respective to bulk value. Fig.6 shows di-

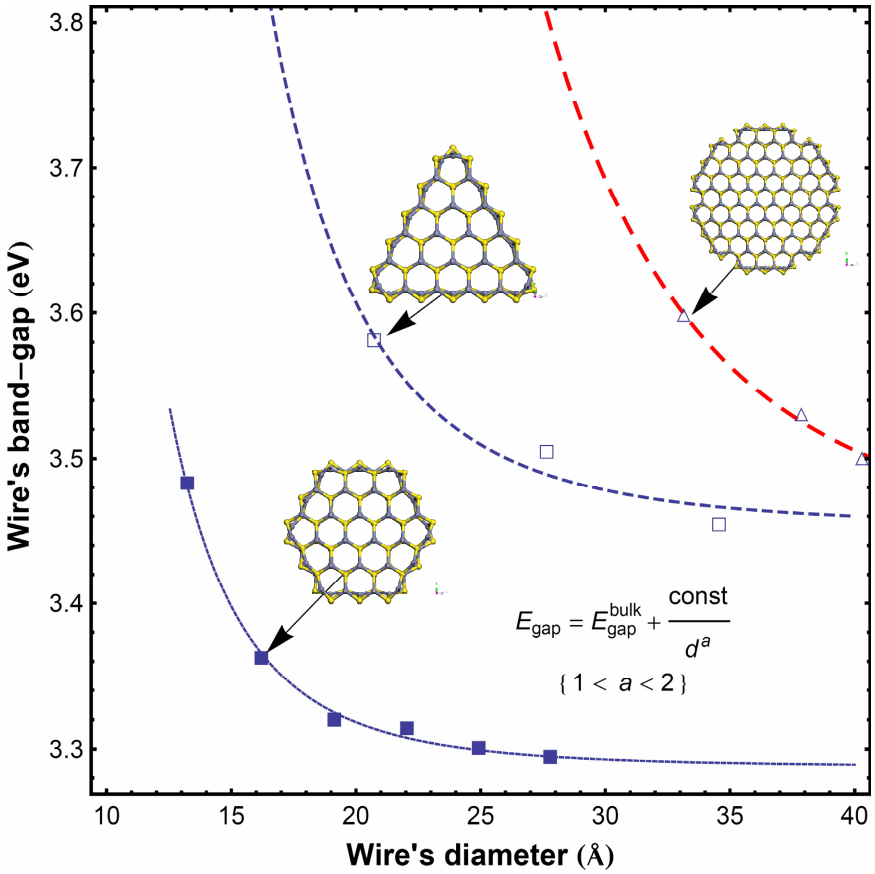

Fig. 6. Wire's band gap vs diameter

ameter dependence of band gap, which is the evident the quantum confinement effect in cross-sectional direction, i.e. wire diameter. The fitting line show the tendency of diameter dependence with characterized by the exponent a, the received value of which is found to be comparable with experiental values [14].

V. CONCLUSIONS

In summary, we have examined the atomistic and electronic structures and stability of nanowire with various shapes of wurzite ZnS grown in [0001] direction of a wide range of diameters $\sim 10 - 40$ Å. The surface relaxations causes the bond strained in length and angle similarly for all studied wire with the strain energy decreasing with increasing wire

diameter. The quantum confinement, expressed here via the wire diameter and the surface relaxation are the two factors that dominate the influence on all wire's characteristics such as band gap, Young's modulus... Our simulation result is agreed well with other theoretical and experimental data.

ACKNOWLEDGMENT

This work was supported by the Vietnamese NAFOSTED program No. 103.02.100.09.

REFERENCES

[1] Xiaosheng Fang, Tianyou Zhai b, Ujjal K. Gautam, Liang Li, Limin Wua, Yoshio Bando, and Dmitri Golberg, *Progress in Materials Science* **56** (2011) 175-287
[2] Matt Law, Joshua Goldberger, and Peidong Yang, *Annual Review of Materials Research* **34** (2004) 83-122.
[3] B. Wang, J. Zhao, J. Jia, D. Shi, J. Wan, G. Wang, and H. Xu, *Appl. Phys. Lett.* **93** (2008) 021918.
[4] Guofeng Wang and Xiaodong Li, *Appl. Phys. Lett.* **91** (2007) 231912.
[5] Y. Maoa, J. Zhonga, Y. Chen, *Physica* **E40** (2008) 499-502.
[6] Y. R. Yang, X. H. Yan, Y. Xiao, Z. H. Guo, *Chem. Phys. Lett.* **446** (2007) 98-102.
[7] M. Elstner, D. Porezag, G. Jungnickel, J. Elsner, M. Haugk, Th. Frauenheim, S. Suhai, and G. Seifert, *Phys. Rev.* **B58** (1998) 7260.
[8] C. Kohler, G. Seifert, and T. Frauenheim, *Chem. Phys.* **309** (2005) 23.
[9] M. Elstner, D. Porezag, G. Jungnickel, J. Elsner, M. Haugk, T.; B. Aradi, B. Hourahine and Th. Frauenheim, *J. Phys. Chem.* **A111** (2007) 5678.
[10] simulation code dftb+ at http://www.dftb-plus.info/
[11] Vu Ngoc Tuoc, *Computational Materials Science* **49** (2010) S161-S169
[12] Ney H. Moreira, Grygoriy Dolgonos, Ba'lint Aradi, Andreia L. da Rosa, and Thomas Frauenheim, *J. Chem. Theory Comput.* **5** (2009) 605-614.
[13] J. Carter, Julian D Gale, Bernard Delley, and Catherine Stampfl, *Phys. Rev.* **B77** (2008) 15349.
[14] Hongxia Chen, DaningShi, JingshanQi, and BaolinWang, *Physica* **E42** (2009) 32-37

Received 01 October 2011.